Blue Aggregation-Induced Emission Luminogens: High External Quantum Efficiencies Up to 3.99% in LED Device, and Restriction of the Conjugation Length through Rational Molecular Design

Jing Huang, Ning Sun, Jie Yang, Runli Tang, Qianqian Li, Dongge Ma,* and Zhen Li**

Great efforts have been devoted to seek novel approaches for constructing blue fluorescent materials, which is one of the most important prerequisites for the commercialization of OLEDs. In recent years, various outstanding luminogens with aggregation-induced emission characteristic exhibit promising applications as emitters, but blue AIE fluorophores with excellent EL performance are still very scarce. Here, five hole-dominated blue AIE molecules are demonstrated by adopting construction approaches of changing linkage modes and increasing intramolecular torsion together, with the aim to restrict conjugation lengths without sacrificing good EL data. Device results show that the novel synthesized materials could be applied as bifunctional materials, namely blue light-emitting and hole-transporting materials, with comparable EL efficiencies, and the $\eta_{C,max}$ and $\eta_{ext,max}$ are up to 8.03 cd A^{-1} and 3.99% respectively, which is among the best EL performance for blue AIE luminogens.

1. Introduction

So far, as the result of the intrinsic large band gap, good blue organic light-emitting materials were still scarce, and critically needed to be explored, to meet the commercialization requirements as red and green counterparts achieved.[1,2] While the efficiencies of organic light-emitting diodes based on blue fluorophors were not high enough, the blue phosphorescent OLEDs (PhOLEDs) with higher efficiencies typically suffered from the poor stability and longevity, in addition to the formidable challenge encountered in the design of efficient blue phosphors.[3,4] Consequently, great efforts have been devoted to seek novel approaches for constructing blue luminogens.

Recently, Adachi et al. have obtained pure blue OLEDs by efficient thermally activated delayed fluorescence materials with external quantum efficiencies up to 9.9%, nearly doubling the theoretical upper limit (5%) for fluorescent devices.[5] This exciting result re-attracted many interests on the pure organic fluorophors.[6,7] On the other hand, from 2001, pioneered by Tang et al., the research of organic fluorophors with the characteristic of aggregation-induced emission (AIE) has become a hot topic.[8–11] And according to Tang's concept for light-emitting materials, the designed AIEgens demonstrated totally different emissive behavior from conventional fluorophores with the notorious aggregation-caused quenching (ACQ) effect in the solid state: a series of propeller-like molecules were turned from faint fluorophores in solution to strong emitters in the aggregation state, derived from the restricted rotation of some aromatic rings. Especially, one typical AIE molecule, 1-methyl-1,2,3,4,5-pentaphenylsilole, demonstrated very high efficiency of 8% in its OLED device.[8,9] The emission color was not blue, but green, possibly due to the relatively long conjugation length of this molecule.[10] Actually, there were few reports concerning the blue AIE fluorophors, once again showing the difficulty to achieve good blue organic light-emitting materials.

Fortunately, in the past several years, by utilizing different linkage modes and increasing the twisting degree of the molecules in the presence of additional groups, we have successfully developed facile approaches to tune the balance of the molecular rotation and conjugation, and construct blue AIE luminogens.[11] The OLED devices clearly demonstrated that their intrinsic band gaps have been efficiently restricted for blue or deep-blue emissions, and the maximum current efficiency is up to 3.74 cd A^{-1}. Is there any more room to further improve the efficiency? Considering the different function of the two design strategies, we are wondering how about the combination of these two methods, perhaps, the effect of "one plus one larger than two" could be realized. Thus, we designed and synthesized a series of AIE molecules, TPA-3*m*TPE, TPA-3MethylTPE, MethylTPA-3*p*TPE, MethylTPA-3*m*TPE and MethylTPA-3MethylTPE (**Chart 1**), by utilizing triphenylamine (TPA) or methyl-substituted TPA as core and tetraphenylethene (TPE) derivatives in peripheries. Indeed, the combination made the conjugation of the five molecules finely tuned

J. Huang, J. Yang, R. Tang, Dr. Q. Li, Prof. Z. Li
Department of Chemistry
Wuhan University
Wuhan 430072, China
E-mail: qianqian-alinda@163.com;
lizhen@whu.edu.cn; lichemlab@163.com
N. Sun, Prof. D. Ma
Institute of Applied Chemistry
The Chinese Academy of Sciences
Changchun 130022, China
E-mail: mdg1014@ciac.jl.cn

DOI: 10.1002/adfm.201401867

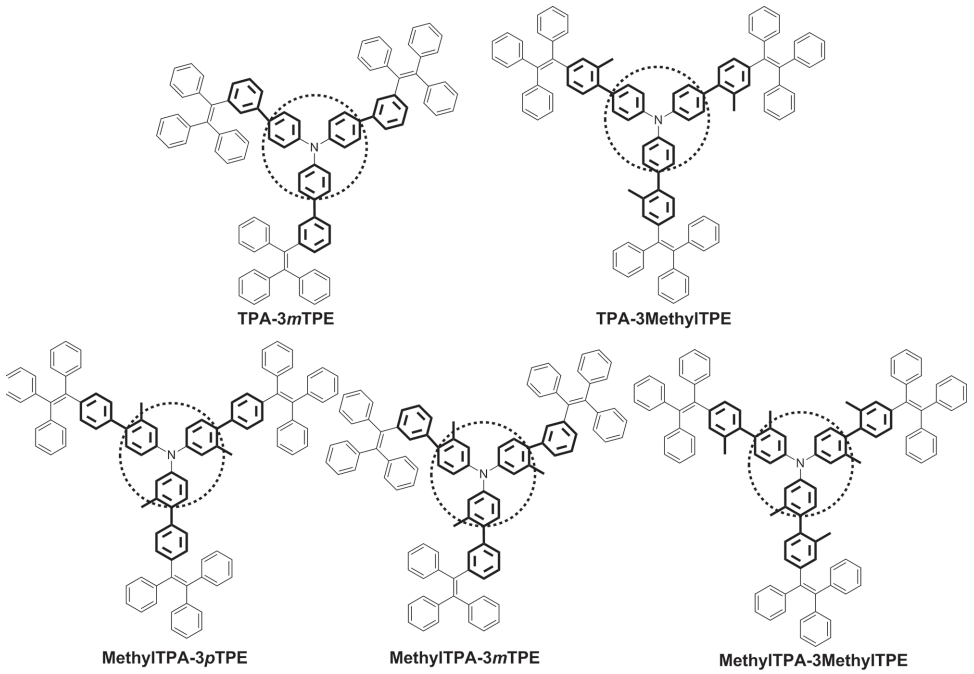

Chart 1. Chemical structures of TPA-3*m*TPE, TPA-3MethylTPE, MethylTPA-3*p*TPE, MethylTPA-3*m*TPE and MethylTPA-3MethylTPE.

for blue emissions, with CIE coordinated blue-shifting to (0.17, 0.19). More excitingly, thanks to the good hole mobility of TPA groups, these luminogens have been demonstrated as hole-transport materials for nondoped OLEDs, in addition to excellent blue fluorescent emitters. The maximum current efficiency and external quantum efficiency of the devices were up to 8.03 cd A^{-1} and 3.99% respectively, demonstrating the superiority of our design concept. Herein, we would like to present their synthesis, thermal, photophysical, electrochemical and EL properties in detail.

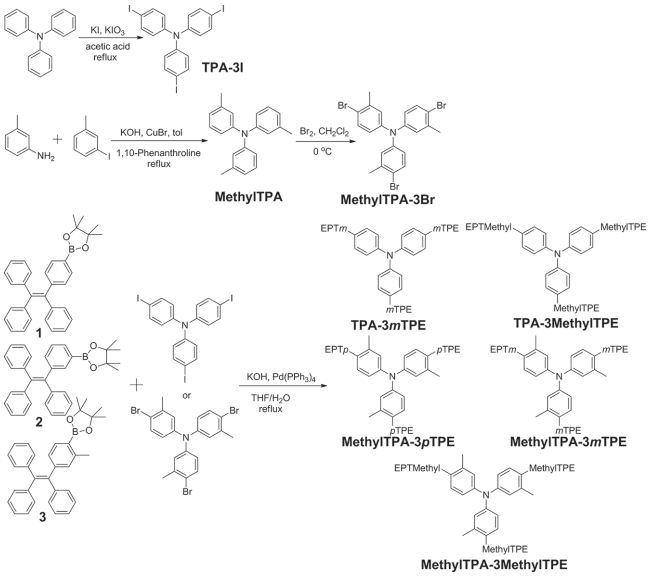

Scheme 1. Synthetic routes to TPA-3*m*TPE, TPA-3MethylTPE, MethylTPA-3*p*TPE, MethylTPA-3*m*TPE and MethylTPA-3MethylTPE.

2. Results and Discussion

2.1. Synthesis

The synthetic routes to TPA-3*m*TPE, TPA-3MethylTPE, MethylTPA-3*p*TPE, MethylTPA-3*m*TPE and MethylTPA-3MethylTPE were illustrated in **Scheme 1**. Compound TPA-3I was synthesized according to the literature.[12] Methyl-substituted TPA core was obtained through Ullman reaction between 3-Methylaniline and 3-Iodotoluene, then it was brominated to yield the key intermediate MethylTPA-3Br. The synthesis of TPE boronic esters **1–3** started from 4-bromobenzophenone, 3-bromobenzophenone and 3-Methyl-4-bromobenzophenone respectively, and were yielded through three steps. The final products were conveniently yielded by the palladium-catalyzed Suzuki coupling reactions of the corresponding aromatic bromide and TPE boronic ester in the yields of 36–78%. They were all purified by column chromatography on silica gel using petroleum ether-dichloromethane as eluent and fully characterized by ^{1}H and ^{13}C NMR, mass spectrometry, and elemental analysis.

2.2. Thermal Properties

Generally, good thermal stability of the emitters is beneficial to the process of vacuum deposition and operating stability of the light-emitting devices. The thermal properties of all the new compounds were investigated by thermogravimetric analysis (TGA) and differential scanning calorimetry (DSC) measurements. As depicted in **Figure 1** and **Table 1**, all the fluorophors are thermally stable with T_d (5% weight loss) values in the range of 446–491 °C, owing to the introduction of the rigid and bulky TPA and TPE units. Generally, compounds with *para*-linkage

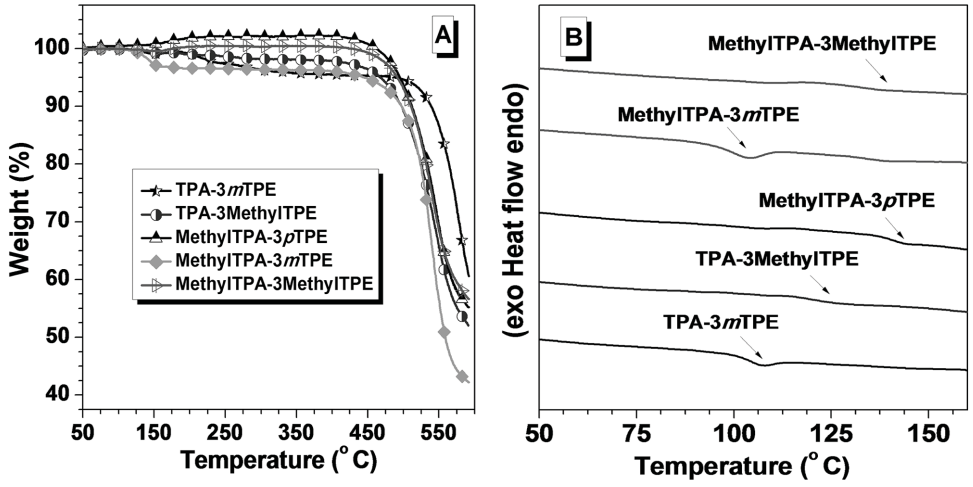

Figure 1. A) TGA and B) DSC curves of TPA-3*m*TPE, TPA-3MethylTPE, MethylTPA-3*p*TPE, MethylTPA-3*m*TPE and MethylTPA-3MethylTPE recorded under N_2 at a heating rate of 10 °C/min.

mode between TPA and TPE units show better thermal stability than the ones with *meta*-linkage way, due to their more rigid conformations. Among them, MethylTPA-3*p*TPE and MethylTPA-3MethylTPE (494 and 491 °C) possess higher decomposition temperatures than other compounds. The glass transition temperatures (T_g) for TPA-3*m*TPE, TPA-3MethylTPE, MethylTPA-3*p*TPE, MethylTPA-3*m*TPE and MethylTPA-3MethylTPE are 107, 129, 144, 104, and 138 °C, respectively, further demonstrating the better thermal stability of MethylTPA-3*p*TPE and MethylTPA-3MethylTPE.

2.3. Optical Properties

All the five molecules have good solubility in common organic solvents, such as dichloromethane, chloroform and tetrahydrofuran (THF) et al., but are insoluble in water. **Figure 2**A shows their absorption spectra in diluted THF solutions. The maximum absorption wavelengths ($\lambda_{abs,max}$) of TPA-3*m*TPE, TPA-3MethylTPE, MethylTPA-3*p*TPE, MethylTPA-3*m*TPE and MethylTPA-3MethylTPE are 337, 341, 342, 321, and 337 nm, respectively. Compared to that of 3TPETPA (370 nm),[5c] the much blue-shifted $\lambda_{max,abs}$, as large as 49 nm, indicates the shorter conjugation of these five luminogens, which is in consistent with our aim of restricting the conjugation extension by changing linkage modes and adding methyl groups. Among them, TPA-3*m*TPE and MethylTPA-3*m*TPE with *meta*-linkage mode between TPE and TPA exhibit more blue-shifted $\lambda_{abs,max}$ than others with *para*-linkage way, also demonstrating that the utilization of *m*TPE unit is more effective than MethylTPE for the tuning of the conjugation length. MethylTPA-3*m*TPE possesses the lowest conjugation degree than the other four compounds, showing its more twisted conformation by employing both construction methods.

In order to study the AIE characteristic of the five TPE-based luminogens, we chose water and THF as the solvent pair for their miscibility and recorded the photoluminescence (PL) change. **Figure 3**A and Figure S1 (Supporting Information) show the PL spectra of the new fluorophores in THF/water mixtures with different water fractions (f_w), which enabled fine-tuning of the solvent polarity and extent of solute aggregation. It is clearly seen that, when molecules were readily dissolved in pure THF solutions, the PL curves are all practically a flat line parallel to the abscissa, showing their faint emission property in

Table 1. The thermal, electrochemical, and photophysical data of TPA-3*m*TPE, TPA-3MethylTPE, MethylTPA-3*p*TPE, MethylTPA-3*m*TPE and MethylTPA-3MethylTPE.

						PL λ_{max}		Φ_F [%]	$\lambda_{max,abs}$
	T_d[a] [°C]	T_g[b] [°C]	E_g[c] [eV]	E_{HOMO}[d] [eV]	E_{LUMO}[e] [eV]	aggr[f] [nm]	film [nm]	aggr[f]	soln[g] [nm]
TPA-3*m*TPE	484	107	3.20	–5.13	–1.93	471	471	33.9	337
TPA-3MethylTPE	468	129	3.12	–5.12	–2.00	485	480	73.9	341
MethylTPA-3*p*TPE	494	144	3.16	–5.07	–1.91	486	487	63.8	342
MethylTPA-3*m*TPE	446	104	3.36	–5.09	–1.73	469	466	59.5	321
MethylTPA-3MethylTPE	491	138	3.32	–5.08	–1.76	472	472	54.7	337

[a]5% weight loss temperature measured by TGA under N_2; [b]Glass-transition temperature measured by DSC under N_2; [c]Band gap estimated from optical absorption band edge of the solution; [d]Calculated from the onset oxidation potentials of the compounds; [e]Estimated using empirical equations $E_{LUMO} = E_{HOMO} + E_g$; [f]Determined in THF:$H_2O$ = 1:99 solution; [g]Observed from absorption spectra in dilute THF solution, 10 μM.

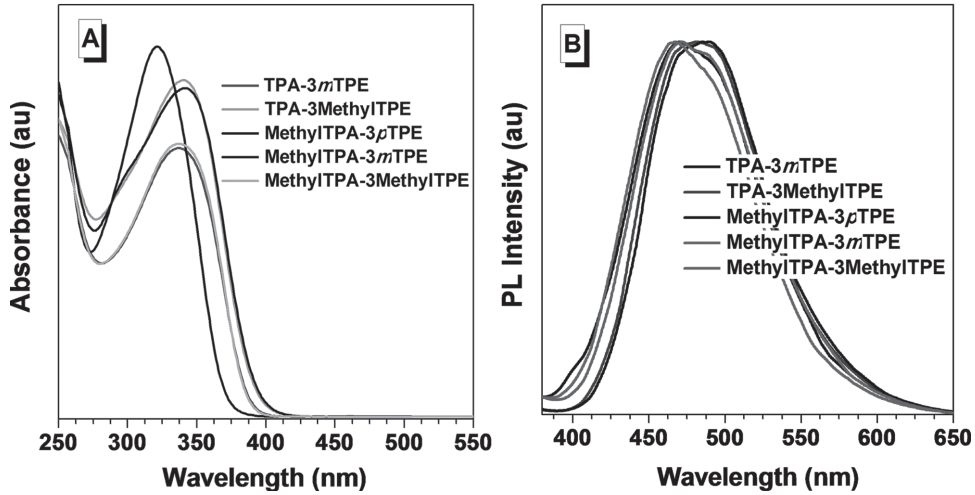

Figure 2. A) UV spectra and B) PL spectra of TPA-3*m*TPE, TPA-3MethylTPE, MethylTPA-3*p*TPE, MethylTPA-3*m*TPE and MethylTPA-3MethylTPE in THF solution (≈10 μM) and in the thin solid films respectively.

the solution state. With gradual addition of water, the PL intensities of the five compounds remain low in aqueous mixtures with water content less than 50%, above which they increase swiftly and clear peaks could be monitored in the emission spectra. From pure THF solution to THF/H_2O mixture with 90% or 95% water content, the emission intensities increase over 350-fold, which could also be verified by visual observations. When illuminated under 365 nm UV lamp, their THF solutions emitted no observable light, but intense emissions were clearly observed from the THF/H_2O mixture with 90% or 95% water content, and the emission maxima are 471, 485, 486, 469 and 472 nm for TPA-3*m*TPE, TPA-3MethylTPE, MethylTPA-3*p*TPE, MethylTPA-3*m*TPE and MethylTPA-3MethylTPE, respectively. However, when more water is added, the emissions of the compounds in aqueous mixtures decrease at some extent, probably due to their relative poor solubility caused by the rigid molecular structures. Moreover, for TPE-*m*TPA and MethylTPA-3*m*TPE, when the water fraction increases from 50 to 90% or 95%, the PL peaks blue-shift from 485 and 489 nm to 471 and 469 nm respectively. This should be probably due to the morphological change of the aggregates from amorphous to crystalline state, which was in consistent with the phenomenon of "crystallization-induced blue emission", as reported in the literature.[13] Thus, this property would contribute to the realization of blue emissions of the corresponding LED devices. The quantitative enhancement of emission was evaluated by the PL quantum yields (Φ_F), using 9,10-diphenylanthracene as the standard. From pure solution in THF to aggregate state in 90% or 95% aqueous mixture, the Φ_F values of TPA-3*m*TPE increased from 0.4% to 33.9%. Similar phenomena were also observed for the other four luminogens. The quantum yields are up to 73.9%, 63.8%, 59.5% and 54.7%, respectively, for

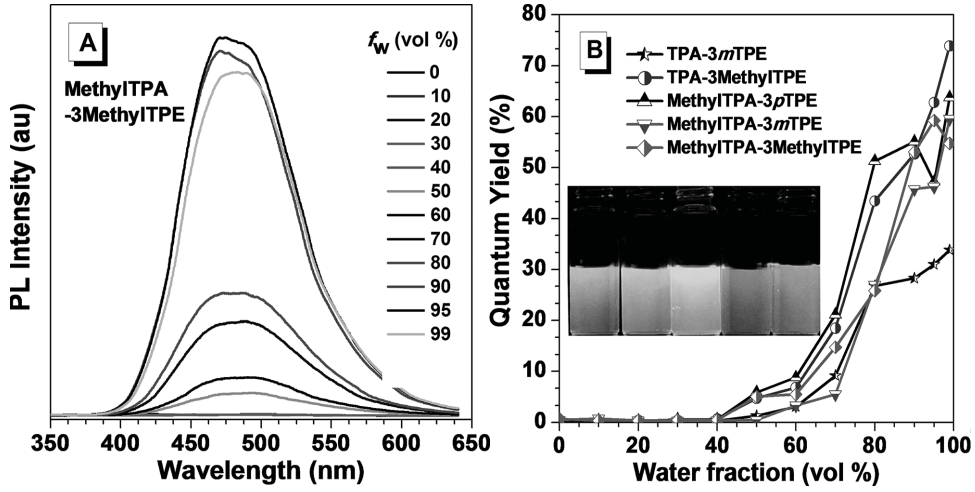

Figure 3. A) PL spectra of MethylTPA-3MethylTPE in THF/H_2O mixtures with different water fractions. Concentration ≈10 μM; excitation wavelength (nm): 330. B) Plots of fluorescence quantum yields determined in THF/H_2O solutions using 9,10-diphenylanthracene (Φ = 90% in cyclohexane) as standard versus water fractions. Inset: photos of the four luminogens in THF/water mixture (f_w = 95%) taken under the illumination of a 365 nm UV lamp.

TPA-3MethylTPE, MethylTPA-3*p*TPE, MethylTPA-3*m*TPE and MethylTPA-3MethylTPE in 90% or 95% aqueous mixture, from being weakly emissive in the solution state.

We further investigated the PL properties of the luminogens in the solid state as luminogenic materials are often fabricated as thin solid films in practical applications. As shown in Figure 2B, all the five derivatives exhibit blue emissions ranging from 466–487 nm, almost the same as the PLs of their aggregates in THF/H_2O mixtures. Among them, the solid-state emission of MethylTPA-3*m*TPE is more blue-shifted than the other four compounds, possibly owing to its more twisted conformation by utilizing *meta*-linkage mode and methyl units together, which is in consistent with our design idea.

2.4. Theoretical Calculations

To further verify the structure-property relationship at molecular level, we have carried out Density Functional Theory (DFT) calculations (B3LYP/6–31g*) of the five luminogens to obtain the optimized structures and orbital distributions of HOMO and LUMO energy levels of TPA-3*m*TPE, TPA-3MethylTPE, MethylTPA-3*p*TPE, MethylTPA-3*m*TPE and MethylTPA-3MethylTPE, respectively. As demonstrated in **Figure 4**, the electron clouds of HOMO energy levels are all mainly located at the central TPA or methyl-substituted TPA core, due to the good electron-donating and hole-transporting abilities of TPA. While the LUMOs of the four chromophores are dominated by orbitals from the TPE peripheries. For TPA-3MethylTPE and MethylTPA-3*p*TPE, the dihedral angles of the adjacent phenyl rings between TPA and TPE units are ≈50°, much smaller than that of MethylTPA-3MethylTPE (≈80°), clearly indicating that the molecular torsion could be effectively increased by adding methyl groups. While for TPA-3*m*TPE and MethylTPA-3*m*TPE, the dihedral angles are ≈38° and 55° respectively, showing the superiority of employing both methods in conjugation tuning. However, it should be noted that not only the dihedral angles of the adjacent phenyl rings of TPA and TPE units, but also the twist degree of the TPE moiety itself, could affect the intramolecular conjugation in a large degree. For example, in MethylTPA-3*m*TPE, the dihedral angle between the TPA and TPE units is 55°, smaller than that of MethylTPA-3MethylTPE (≈80°). However, the twisting degree of TPE itself is higher in the former one, which will result in the shorter whole conjugation length of the molecule. This directly leads to the blue-shifted emission of MethylTPA-3*m*TPE, being in consistent with its shorter absorption maximum wavelength (321 nm) than those of others (337–342 nm).

2.5. Electrochemical Properties

Cyclic voltammetry (CV) measurements were carried out to investigate the electrochemical properties of the five AIE fluorophores. The highest occupied molecular orbital (HOMO) energy levels were estimated from the onset oxidation potentials according to the equation: HOMO = –(4.8 + E_{ox}) eV, while the lowest unoccupied molecular orbital (LUMO) energy levels were obtained from optical band-gap energies (estimated from the onset wavelengths of the UV absorptions) and HOMO values. As shown in Figure S2 (Supporting Information) and Table 1, for TPA-3*m*TPE, TPA-3MethylTPE, MethylTPA-3*p*TPE, MethylTPA-3*m*TPE and MethylTPA-3MethylTPE, their HOMO values were calculated to be –5.13, –5.12, –5.07, –5.09, and –5.08 eV, respectively, which are slightly higher than that of NPB (–5.30 eV). This suggests that all the five molecules might possess good hole-transporting property, mainly due to the fine contribution from the TPA and TPE units.[14] Their corresponding LUMO energy levels were calculated to be –1.93, –2.00, –1.91, –1.73 eV, and –1.76 eV, respectively. The small energy gap between emissive layer and the hole-transporting layer suggests the efficient charge transfer in the OLEDs, thus low turn-on voltage and high luminescence of the device. Moreover, the larger band-gap of MethylTPA-3*m*TPE (3.21 eV) has

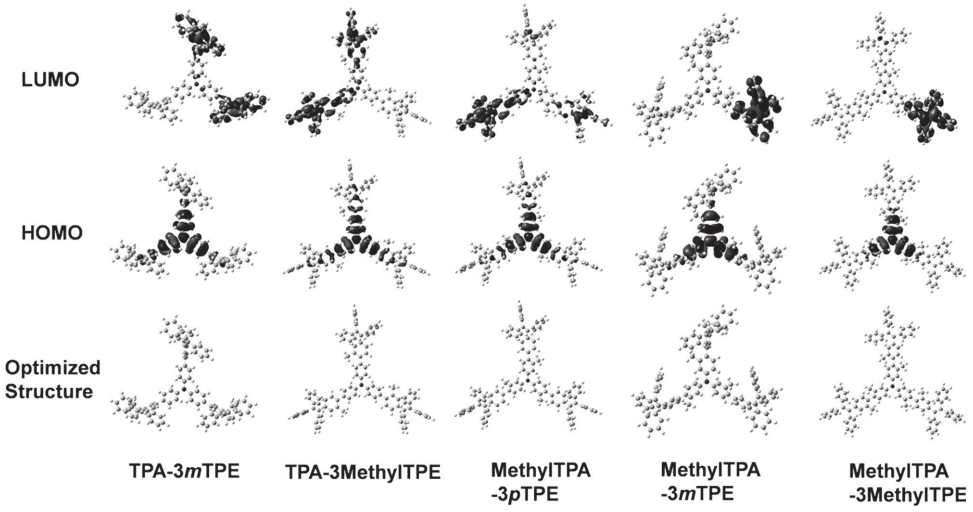

Figure 4. Calculated molecular orbital amplitude plots of HOMO and LUMO levels and optimized molecular structures of TPA-3*m*TPE, TPA-3MethylTPE, MethylTPA-3*p*TPE, MethylTPA-3*m*TPE and MethylTPA-3MethylTPE.

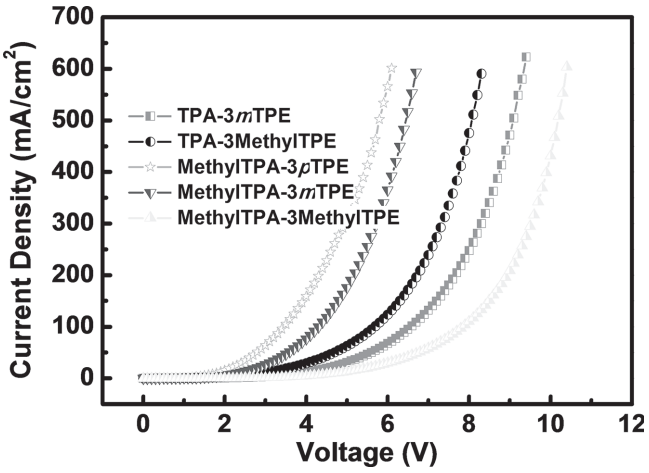

Figure 5. Current density–voltage characteristics of hole-only devices of TPA-3*m*TPE, TPA-3MethylTPE, MethylTPA-3*p*TPE, MethylTPA-3*m*TPE and MethylTPA-3MethylTPE with a configuration of ITO/MoO_3 (10 nm)/X(75 nm)/MoO_3 (10 nm)/Al.

demonstrated its shorter effective conjugation, owing to its more twisted conformation by adopting *m*TPE and methyl-substituted TPA together.

2.6. Electroluminescence

Efficient solid state emission and good charge transport ability are two requisite factors for desirable blue emitters. Although OLEDs with multilayers have been fabricated to balance the carrier injection and transport, simplified device configurations will be more valuable in real applications. Inspired by the efficient solid state emission and high-lying HOMO energy levels derived from TPA moieties, the novel synthesized materials were applied as bifunctional materials, namely blue light-emitting and hole-transporting materials. To preliminarily evaluate the hole-transporting ability of the five compounds, hole-only devices with a configuration of ITO/MoO_3 (10 nm)/X(75 nm)/MoO_3 (10 nm)/Al were fabricated and characterized. In these devices, MoO_3 worked as hole-injection and electron-blocking layers, and X refers to TPA-3*m*TPE, TPA-3MethylTPE, MethylTPA-3*p*TPE, MethylTPA-3*m*TPE or MethylTPA-3MethylTPE. **Figure 5** shows their current density-voltage (*J*–*V*) characteristics, and it can be seen that all the devices display good hole-transporting property. Among them, device based on MethylTPA-*p*TPE exhibits higher current density at a given applied voltage, indicating MethylTPA-*p*TPE possesses better hole-transporting ability than the other four compounds. It is possibly due to its more planar conformation, which is beneficial for carrier transport. Moreover, we have also fabricated hole-only device of NPB as a reference. As shown in Supporting Information Figure S5, it is observed that the hole mobility of NPB is inferior to that of MethylTPA-3*p*TPE and MethylTPA-3*m*TPE, and comparable with that of TPA-3MethylTPE, demonstrating the superiority of the design tactics and good device performance of the target molecules.

To investigate the light-emitting behaviors of the five luminogens, multilayer OLEDs (A-E) with a configuration of ITO/MoO_3 (10 nm)/NPB (60 nm)/X(15 nm)/TPBi (35 nm)/LiF(1 nm)/Al were fabricated, in which MoO_3, NPB and TPBi worked as the hole-injection, hole-transporting and hole-blocking layers, respectively, and X (TPA-3*m*TPE, TPA-3MethylTPE, MethylTPA-3*p*TPE, MethylTPA-3*m*TPE or MethylTPA-3MethylTPE) served as emitters. Supporting Information Figure S3 shows the current density-voltage-brightness (*J*–*V*–*L*) characteristics, current efficiency versus current density curves, and EL spectra of the OLEDs. As listed in **Table 2**, all the devices turn on at a low voltage from 2.9 to 3.1 V, showing the small injection barriers between transporting layers and emitters. It should be ascribed to the employment of hole-dominated TPA units, which impart the target molecules with hole-transport nature. Accompanying with the increase of the voltage, the luminance increases rapidly. Generally, emitters with MethylTPE moieties peripheries exhibit better EL performance than the ones adopting *m*TPE units. Devices based on TPA-3*m*TPE and MethylTPA-3*m*TPE exhibit lower EL efficiencies with maximum luminance (L_{max}) of 6636 and 6348 cd m^{-2},

Table 2. EL performances (devices A-E with HTL and devices a-e without HTL) of TPA-3*m*TPE (A and a), TPA-3MethylTPE (B and b), MethylTPA-3*p*TPE (C and c), MethylTPA-3*m*TPE (D and d), and MethylTPA-3MethylTPE (E and e).[a)]

Device	λ_{EL} [nm]	V_{on} [V]	L_{max} [cd m^{-2}]	$\eta_{P,max}$ [lm w^{-1}]	$\eta_{C,max}$ [cd A^{-1}]	$\eta_{ext,max}$ [%]	CIE[b)] [*x*,*y*]
A	479	3.1	6636	2.62	3.08	1.66	0.17, 0.24
a	470	3.1	6230	3.31	3.45	1.95	0.17, 0.22
B	470	2.9	19023	6.17	7.05	3.70	0.17, 0.25
b	472	2.9	15235	6.63	6.20	3.27	0.17, 0.25
C	480	3.1	13639	7.04	8.03	3.99	0.17, 0.28
c	469	2.9	15089	6.88	6.51	3.39	0.18, 0.25
D	459	3.1	6348	2.20	2.58	1.64	0.17, 0.19
d	459	3.1	4989	2.26	2.49	1.54	0.17, 0.19
E	469	3.1	10709	5.03	5.46	3.06	0.17, 0.22
e	474	3.3	8271	5.59	6.24	3.29	0.16, 0.25

[a)]Abbreviations: V_{on} = turn-on voltage at 1 cd m^{-2}, L_{max} = maximum luminance, $\eta_{C,max}$, $\eta_{C,max}$ and $\eta_{ext,max}$ = maximum power, current and external efficiencies, respectively; [b)]CIE = Commission International de l'Eclairage coordinates at 100 mA/cm^2.

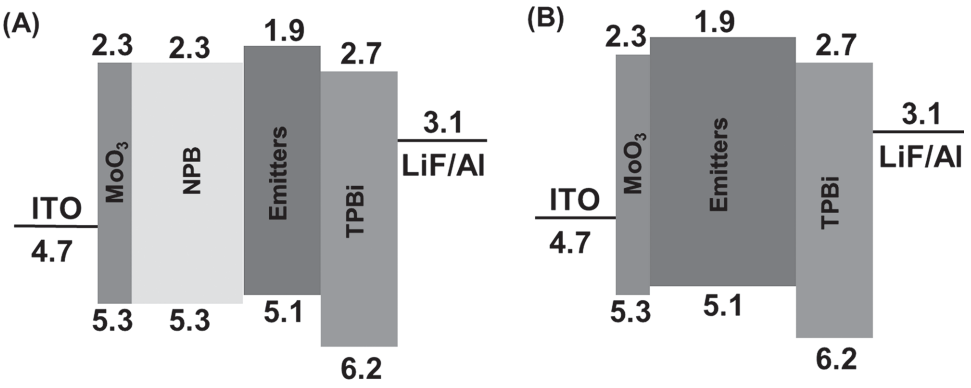

Figure 6. A) EL devices with HTL and B) EL devices without HTL. Abbreviations: NPB = 4,4-bis(1-naphthylphenylamino)biphenyl, TPBi = 1,3,5-tris(N-phenylbenzimidazol-2-yl)benzene, Emitters = TPA-3*m*TPE, TPA-3MethylTPE, MethylTPA-3*p*TPE, MethylTPA-3*m*TPE or MethylTPA-3MethylTPE.

maximum current efficiency ($\eta_{C,max}$) of 3.08 and 2.58 cd A^{-1}, and maximum power efficiency ($\eta_{P,max}$) of 2.26 and 2.20 lm W^{-1} respectively. However, their EL emissions still retain in the blue region with CIE coordinates of (0.17, 0.24) and (0.17, 0.19), compared to 3TPETPA with green emission. It should be ascribed to the *meta*-linkage way between TPA and TPE units, which effectively controls the conjugation extension of the adducts. Moreover, we chose methyl unit as the additional group for generating molecular distortion, because according to our previous research, the dihedral angle of two phenyl rings is almost perpendicular when modifying methyl groups at their 2,2′-positions without bringing about redundant conjugation. For MethylTPA-3*m*TPE, it was constructed by employing both methods of changing linking positions and causing molecular distorsion. As a result, its EL emission is more blue-shifted.

Better EL data were obtained for TPA-3MethylTPE and MethylTPA-3MethylTPE with L_{max}, $\eta_{C,max}$ and $\eta_{P,max}$ of 19023 and 10709 cd m^{-2}, 7.05 and 5.46 cd A^{-1}, and 6.17 and 5.03 lm W^{-1} respectively. Their EL emissions are slightly red-shifted than that of MethylTPA-3*m*TPE, with CIE coordinates of (0.17, 0.25) and (0.17, 0.22). Among them, MethylTPA-3*p*TPE possesses the best EL performance with L_{max}, $\eta_{C,max}$, $\eta_{P,max}$ and $\eta_{ext,max}$ of 13639 cd m^{-2}, 8.03 cd A^{-1}, 7.04 lm W^{-1} and 3.99%, which is in consistent with its more planar conformation and better hole transporting property. As discussed in the introduction part, to construct blue AIE luminogens, there is a balance between blue emission and good device performance. Generally, the better intramolecular conjugation, the better performance, however, the longer maximum emission wavelength. For MethylTPA-*p*TPE, although it possessed moderate PLQY and similar energy levels with the other molecules, its more planar conformation was beneficial for charge transport, and the incorporation of methyl groups and the *para*-linkage way ensured the blue emission of MethylTPA-*p*TPE. As shown in Table 2, the CIE value of MethylTPA-*p*TPE is a little higher than those of others, indicating its better intramolecular conjugation, as a result, MethylTPA-*p*TPE exhibited the best performance. In comparison with 3TPETPA (CIE coordinates of (0.19, 0.32)), the EL spectra of the five molecules are all blue-shifted to blue or sky-blue region without sacrificing good device performance and stability.

To further explore the hole-transporting characteristic of the five compounds, typical two-layer devices (a–e) with ITO/MoO_3 (10 nm)/X(75 nm)/TPBi(35 nm)/LiF(1 nm)/Al were also fabricated for comparison, in which hole-transporting layer (HTL) NPB was eliminated, and X served both as hole-transporting material and emitters. **Figure 6** shows the energy diagram and configurations of these two kinds of devices. When compared to devices A-E (**Figure 7** and Supporting Information Figure S3), devices a-e without HTL also show low turn-on voltages (2.9–3.3 V), as depicted in Figure S4 (Supporting Information) and **Figure 8**, indicating the balanced carrier injection and transporting originated from the excellent hole-transporting ability of the emitters. This helps to simplify the device configurations, which is more valuable in practical applications. Excitingly, as demonstrated in Table 2, most of the devices show only slight decrease in the EL efficiencies, and some even possess better EL performance than the ones with NPB layer. For example, the device based on MethylTPA-3*p*TPE exhibits better EL efficiencies with L_{max}, $\eta_{C,max}$ and $\eta_{P,max}$ of 15089 cd m^{-2}, 6.51 cd A^{-1}, and 6.88 lm W^{-1} respectively, which is comparable with those obtained from standard device. Also for MethylTPA-3MethylTPE, it possesses better EL performance in the device without HTL. It evidently shows that all the new AIE molecules could be used both as blue light-emitting and hole-transporting materials, realizing our synthetic idea of generating functional blue AIE luminogens by facilely changing linkage modes and increasing molecular torsion.

Interestingly, the efficiency and color purity of device A and C were inferior to those of device a and c utilizing TPA-3*m*TPE and MethylTPA-3*p*TPE as hole-transporting and emissive layer. It can be assumed that the charge recombination zone formed near the interface of NPB and the emitting layer, which may lead to the formation of an exciplex at the interface for device A and C and harm the color purity, resulting in the little red-shifted EL spectrum of device A and C compared to those of device a and c. The results suggest that TPA-3*m*TPE and MethylTPA-3*p*TPE can play a better role in hole-injection and transporting than NPB. While for MethylTPA-3MethylTPE with the highest LUMO levels (devices E and e), it possesses the worst hole-transport ability. After removing the hole-transport layer, the recombination zone may be restrained in the emissive layer, leading to the improved device performance and a little red-shifted EL emission (5 nm).

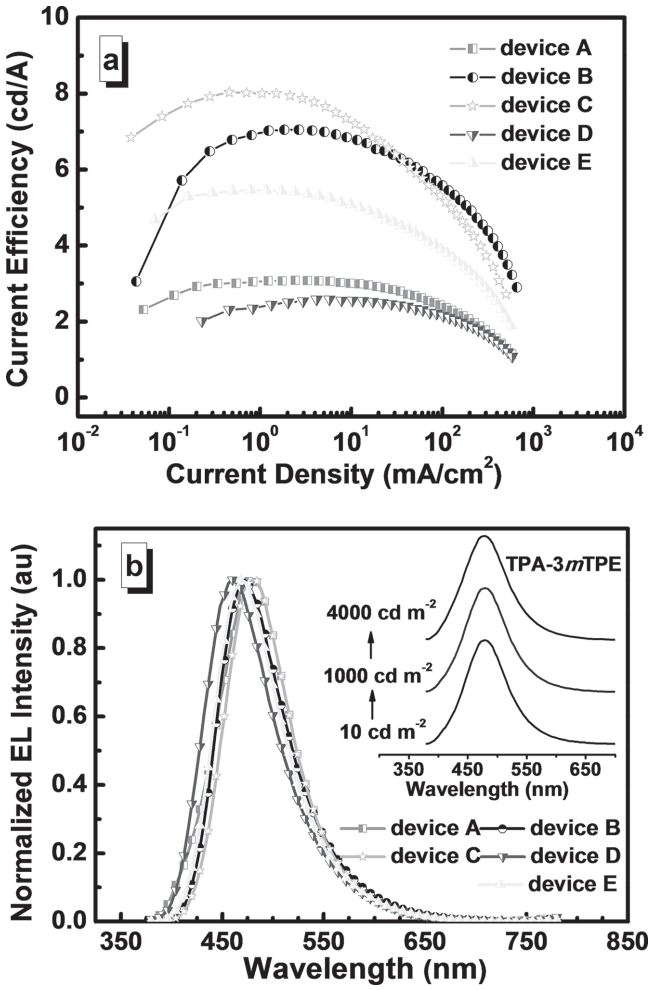

Figure 7. a) Change in current efficiency with the current density in multilayer EL devices (with HTL) of TPA-3*m*TPE (A), TPA-3MethylTPE (B), MethylTPA-3*p*TPE (C), MethylTPA-3*m*TPE (D), or MethylTPA-3MethylTPE (E). b) EL spectra of the luminogens. Device configurations: ITO/MoO_3 (10 nm)/NPB (60 nm)/EML (15 nm)/TPBi (35 nm)/LiF (1 nm)/Al. Inset (b): TPA-3*m*TPE-based device viewed in the normal direction at a luminance of 10, 1000, and 4000 cd m^{-2}.

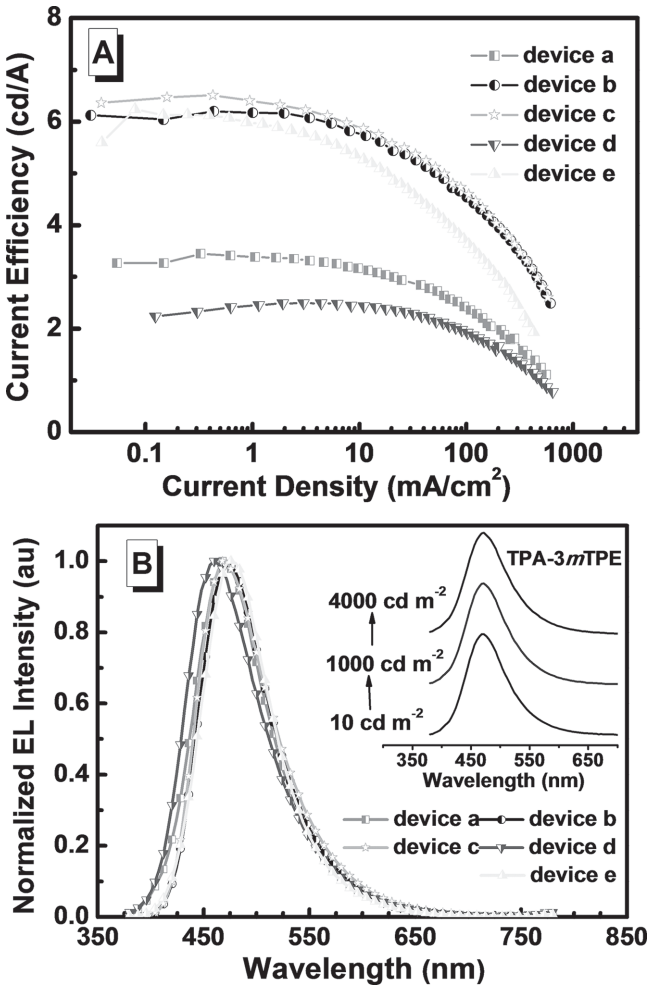

Figure 8. A) Change in current efficiency with the current density in multilayer EL devices (without HTL) of TPA-3*m*TPE (a), TPA-3MethylTPE (b), MethylTPA-3*p*TPE (c), MethylTPA-3*m*TPE (d) or MethylTPA-3MethylTPE (e). B) EL spectra of the luminogens. Device configurations: ITO/MoO_3 (10 nm)/EML (75 nm)/TPBi (35 nm)/LiF (1 nm)/Al. Inset of (B): TPA-3*m*TPE-based device viewed in the normal direction at a luminance of 10, 1000, and 4000 cd m^{-2}.

3. Conclusions

In this work, we have successfully synthesized five novel AIE molecules, namely TPA-3*m*TPE, TPA-3MethylTPE, MethylTPA-3*p*TPE, MethylTPA-3*m*TPE and MethylTPA-3MethylTPE, with the aim of generating functional blue AIE emitters and simplifying device configurations. By incorporating the hole-dominated TPA or methyl-substituted TPA moieties, the target molecules exhibit excellent hole-transporting property, which are verified by the hole-only devices. Moreover, the π-conjugation lengths of the five luminogens have been effectively restricted by adopting *meta*-TPE units and adding methyl groups. When fabricated as emitters in OLEDs with or without hole-transporting layers, all the emitters exhibit blue emissions and comparable EL performance with $\eta_{C,max}$ and $\eta_{ext,max}$ up to 8.03 cd A^{-1} and 3.99%, evidently showing their bifunctional property of serving both as emitters and hole-transporting materials. The excellent EL data are much higher than those we have previously obtained, and also among the best EL performance for blue AIE luminogens, strongly indicating the significant construction methods for conjugation tuning by changing linkage modes and increasing molecular torsion. Enlightened by the successful adoption of TPA units, it is anticipated that more AIE emitters with hole-, electron- or ambipolar transporting characteristic could be developed by ingeniously incorporating functional groups, thus our further work will focus on constructing functional deep-blue AIE emitters with improved EL efficiencies by employing these facile synthetic strategies.

4. Experimental Section

Characterization: ^{1}H and ^{13}C NMR spectra were measured on a MECUYRVX300 spectrometer. Elemental analyzes of carbon, hydrogen, and nitrogen were performed on a CARLOERBA-1106 microanalyzer. Mass spectra were measured on a ZAB 3F-HF spectrometer.

High-resolution mass spectra (HR-MS) were recorded on a JEOL LMS-HX-110 spectrometer with 3-nitrobenzyl alcohol (NBA) as a matrix. UV–Vis absorption spectra were recorded on a Shimadzu UV-2500 recording spectrometer. Photoluminescence spectra were recorded on a Hitachi F-4500 fluorescence spectrometer. Differential scanning calorimetry (DSC) was performed on a Mettler Toledo DSC 822e at a heating and cooling rate of 15 °C min^{-1} from room temperature to 180 °C under nitrogen. The glass transition temperature (T_g) was determined from the second heating scan. Thermogravimetric analysis (TGA) was undertaken with a NETZSCH STA 449C instrument. The thermal stability of the samples under a nitrogen atmosphere was determined by measuring their weight loss while heating at a rate of 10 °C min^{-1} from 25 to 600 °C. Cyclic voltammetry (CV) was carried out on a CHI voltammetric analyzer in a three-electrode cell with a Pt counter electrode, a Ag/AgCl reference electrode, and a glassy carbon working electrode at a scan rate of 100 mV s^{-1} with 0.1 M tetrabutylammonium perchlorate (purchased from Alfa Aesar) as the supporting electrolyte, in anhydrous dichloromethane solution purged with nitrogen. The potential values obtained in reference to the Ag/Ag^+ electrode were converted to values versus the saturated calomel electrode (SCE) by means of an internal ferrocenium/ferrocene (Fc^+/Fc) standard.

Computational Details: The geometrical and electronic properties were optimized at B3LYP/6–31g(d) level using Gaussian 09 program. The molecular orbitals were obtain at the same level of theory.

Preparation of Nanoaggregates: Stock THF solutions of the fluorophores were prepared with a concentration of 10^{-3} mol/L. Aliquots of the stock solution were transferred to 10 mL colorimetric cylinders. Then appropriate amounts of THF and water were added successively under vigorous shaking to furnish 10^{-5} M solutions with different water fractions (0–99.9 vol%). The PL measurements of the resultant solutions were then performed immediately.

OLED Device Fabrication and Measurement: The hole-transporting material NPB (1,4-bis(1-naphthylphenylamino)-biphenyl) and electron-transporting material 1,3,5-tris(*N*-phenylbenzimidazol-2-yl)benzene (TPBI) were obtained from a commercial source. The EL devices were fabricated by vacuum deposition of the materials at a base pressure of 10^{-6} Torr onto glass precoated with a layer of indium tin oxide (ITO) with a sheet resistance of 25 Ω per square. Before deposition of an organic layer, the clear ITO substrates were treated with oxgen plasma for 2 min. The deposition rate of organic compounds was 1–2 Å s^{-1}. Finally, a cathode composed of lithium fluoride (1 nm) and aluminium (100 nm) was sequentially deposited onto the substrate in the vacuum of 10^{-6} Torr. The *L–V–J* of the devices was measured with a Keithey 2400 Source meter and a Keithey 2000 Source multimeter equipped with a calibrated silicon photodiode. The EL spectra were measured by JY SPEX CCD3000 spectrometer. All measurements were carried out at room temperature under ambient conditions.

Preparation of Compounds: All other chemicals and reagents were obtained from commercial sources and used as received without further purification. Solvents for chemical synthesis were purified according to the standard procedures.

Synthesis of MethylTPA: A mixture of compound 3-Methylaniline (536 mg, 5 mmol), 3-Iodotoluene (2.73 g, 12.5 mmol) and 1,10-Phenanthroline monohydrate (200 mg, 1 mmol) in toluene (20 mL) was heated at 100 °C under nitrogen. After 10 min, potassium hydroxide and cuprous bromide were added to the solution successively and refluxed overnight. Then, the reaction was quenched with water and the mixture was extracted with dichloromethane. The organic layer was combined and dried with anhydrous sodium sulfate. After filtration and solvent evaporation, the crude product was purified by silica gel column chromatography using petroleum ether/dichloromethane as eluent. White powder of MethylTPA was obtained in the yield of 37% (105 mg). ^{1}H NMR (300 MHz, $CDCl_3$) δ (ppm): 7.15–7.10 (m, 3H), 6.89–6.83 (m, 5H), 6.83–6.80 (m, 4H), 2.25 (s, 9H).

Synthesis of MethylTPA-3Br: MethylTPA (3.7 g, 12.9 mmol) was dissolved in unhydrous dichloromethane (70 mL) at 0 °C under nitrogen, to which bromine (6.3 g, 39.3 mmol) was added dropwise and the mixture stirred for a further 0.5 h. After removing the solvent the solid was refluxed in hot methanol (80 mL) for 1 h and recrystallized in methanol and THF. White powder of MethylTPA-3Br was obtained in the yield of 62% (4.2 g). ^{1}H NMR (300 MHz, $CDCl_3$) δ (ppm): 7.39–7.36 (d, J = 8.1 Hz, 3H), 6.90–6.89 (m, 3H), 6.75–6.71 (m, 3H), 2.29 (s, 9H).

Synthesis of TPA-3mTPE: A mixture of compound 2 (570 mg, 1.24 mmol), TPA-3I (250 mg, 0.4 mmol), $Pd(PPh_3)_4$ (30 mg) and potassium carbonate (828 mg, 6 mmol) in THF (15 mL) and distilled water (5 mL) was refluxed for 24 h under nitrogen in a 50 mL schlenk tube. The mixture was extracted with dichloromethane. The combined organic extracts were dried over anhydrous Na_2SO_4 and concentrated by rotary evaporation. The crude product was purified by column chromatography on silica gel using dichloromethane/petroleum ether as eluent to afford the product as white powder in the yield of 36% (180 mg). ^{1}H NMR (300 MHz, $CDCl_3$) δ (ppm): 7.20–7.18 (m, 5H), 7.10–7.08 (m, 50H), 7.04–6.95 (m, 14H). ^{13}C NMR (100 MHz, $CDCl_3$) δ (ppm): 146.8, 144.1, 144.0, 143.8, 143.7, 141.4, 141.1, 139.8, 135.6, 131.5, 130.4, 130.3, 130.0, 128.3, 128.0, 127.8, 127.6, 126.7, 124.9, 124.4. HRMS, m/z: 1235.50 ([M^+], calcd for $C_{96}H_{69}N$, 1235.54). Anal. Calcd for $C_{96}H_{69}N$: C, 93.24; H, 5.62; N, 1.13. Found: C, 93.13; H, 5.55; N, 1.08.

Synthesis of TPA-3MethylTPE: A mixture of compound 3 (586 mg, 1.24 mmol), TPA-3I (496 mg, 1.21 mmol), $Pd(PPh_3)_4$ (30 mg) and potassium carbonate (828 mg, 6 mmol) in THF (15 mL) and distilled water (5 mL) was refluxed for 24 h under nitrogen in a 50 mL schlenk tube. The mixture was extracted with dichloromethane. The combined organic extracts were dried over anhydrous Na_2SO_4 and concentrated by rotary evaporation. The crude product was purified by column chromatography on silica gel using dichloromethane/petroleum ether as eluent to afford the product as white powder in the yield of 41% (210 mg). ^{1}H NMR (300 MHz, $CDCl_3$) δ (ppm): 7.21–7.18 (m, 7H), 7.15–7.00 (m, 59H), 7.00–6.97 (m, 3H), 6.89 -6.88 (m, 7H), 2.14 (s, 9H). ^{13}C NMR (100 MHz, $CDCl_3$) δ (ppm): 146.4, 144.0, 142.4, 141.0, 139.6, 136.2, 134.5, 133.6, 131.6, 131.5, 130.3, 129.2, 129.1, 127.8, 126.6, 123.7, 20.8. HRMS, m/z: 1277.57 ([M^+], calcd for $C_{99}H_{75}N$, 1277.59). Anal. Calcd for $C_{99}H_{75}N$: C, 92.99; H, 5.91; N, 1.10. Found: C, 92.56; H, 6.16; N, 1.37.

Synthesis of MethylTPA-3pTPE: A mixture of compound 1 (570 mg, 1.24 mmol), MethylTPA-3Br (210 mg, 0.4 mmol), $Pd(PPh_3)_4$ (30 mg) and potassium carbonate (828 mg, 6 mmol) in THF (15 mL) and distilled water (5 mL) was refluxed for 24 h under nitrogen in a 50 mL schlenk tube. The mixture was extracted with dichloromethane. The combined organic extracts were dried over anhydrous Na_2SO_4 and concentrated by rotary evaporation. The crude product was purified by column chromatography on silica gel using dichloromethane/petroleum ether as eluent to afford the product as white powder in the yield of 51% (260 mg). ^{1}H NMR (300 MHz, $CDCl_3$) δ (ppm): 7.11–7.10 (m, 47H), 7.07–7.05 (m, 22H), 7.00–6.95 (m, 7H), 2.16 (s, 9H). ^{13}C NMR (100 MHz, $CDCl_3$) δ (ppm): 146.8, 144.0, 143.9, 143.8, 142.0, 141.2, 141.0, 139.7, 136.4, 136.1, 131.5, 131.1, 130.6, 128.7, 127.8, 126.6, 125.9, 121.7, 20.8. HRMS, m/z: 1277.59 ([M^+], calcd for $C_{99}H_{75}N$, 1277.59). Anal. Calcd for $C_{99}H_{75}N$: C, 92.99; H, 5.91; N, 1.10. Found: C, 92.37; H, 5.70; N, 1.32.

Synthesis of MethylTPA-3mTPE: A mixture of compound 2 (570 mg, 1.24 mmol), MethylTPA-3Br (210 mg, 0.4 mmol), $Pd(PPh_3)_4$ (30 mg) and potassium carbonate (828 mg, 6 mmol) in THF (15 mL) and distilled water (5 mL) was refluxed for 24 h under nitrogen in a 50 mL schlenk tube. The mixture was extracted with dichloromethane. The combined organic extracts were dried over anhydrous Na_2SO_4 and concentrated by rotary evaporation. The crude product was purified by column chromatography on silica gel using dichloromethane/petroleum ether as eluent to afford the product as white powder in the yield of 78% (400 mg). ^{1}H NMR (300 MHz, $CDCl_3$) δ (ppm): 7.18–7.00 (m, 66H), 6.87–6.83 (m, 10H), 1.82 (m, 9H). ^{13}C NMR (100 MHz, $CDCl_3$) δ (ppm): 146.9, 144.1, 144.0, 143.7, 141.4, 141.3, 141.2, 136.6, 136.3, 132.9, 131.8, 131.7, 130.8, 129.8, 128.1, 128.0, 127.7, 126.7, 125.8, 121.7, 20.7. HRMS, m/z: 1277.56 ([M^+], calcd for $C_{99}H_{75}N$, 1277.59). Anal. Calcd for $C_{99}H_{75}N$: C, 92.99; H, 5.91; N, 1.10. Found: C, 92.75; H, 5.80; N, 1.00.

Synthesis of MethylTPA-3MethylTPE: A mixture of compound 3 (570 mg, 1.24 mmol), MethylTPA-3Br (210 mg, 0.4 mmol), $Pd(PPh_3)_4$ (30 mg) and potassium carbonate (828 mg, 6 mmol) in THF (15 mL)

and distilled water (5 mL) was refluxed for 24 h under nitrogen in a 50 mL schlenk tube. The mixture was extracted with dichloromethane. The combined organic extracts were dried over anhydrous Na_2SO_4 and concentrated by rotary evaporation. The crude product was purified by column chromatography on silica gel using dichloromethane/petroleum ether as eluent to afford the product as white powder in the yield of 57% (300 mg). ^{1}H NMR (300 MHz, $CDCl_3$) δ (ppm): 7.13–7.10 (m, 33H), 7.07–7.06 (m, 24H), 7.00–6.96 (m, 10H), 6.90 -6.86 (m, 14H), 1.91 (s, 18H). ^{13}C NMR (100 MHz, $CDCl_3$) δ (ppm): 146.8, 144.1, 143.9, 143.8, 142.4, 141.2, 141.0, 139.7, 136.9, 135.9, 135.4, 132.8, 131.6, 130.1, 129.1, 128.6, 127.8, 127.6, 126.6, 126.5, 121.3, 20.0. TOF, m/z: 1318.5158 ([M^+], calcd for $C_{102}H_{81}N$, 1319.6369). Anal. Calcd for $C_{102}H_{81}N$: C, 92.76; H, 6.18; N, 1.06. Found: C, 92.90; H, 6.45; N, 1.01.

Supporting Information

Supporting Information is available from the Wiley Online Library or from the author.

Acknowledgements

J.H. and N.S. contributed equally to this work. The authors are grateful to the National Fundamental Key Research Program (2013CB834701, 2013CB834805), and the National Science Foundation of China (no. 21325416, 21161160556, 51333007) for financial support.

Received: June 7, 2014
Revised: August 10, 2014
Published online: October 13, 2014

[1] a) C. W. Tang, S. A. Vanslyke, *Appl. Phys. Lett.* **1987**, *51*, 913; b) K. T. Kamtekar, A. P. Monkman, M. R. Bryce, *Adv. Mater.* **2010**, *22*, 572.
[2] a) G. M. Farinola, R. Ragni, *Chem. Soc. Rev.* **2011**, *40*, 3467; b) M. C. Gather, A. Kohnen, K. Meerholz, *Adv. Mater.* **2011**, *23*, 233.
[3] a) E. Holder, B. M. W. Langeveld, U. S. Schubert, *Adv. Mater.* **2005**, *17*, 1109; b) Y. Chi, P.-T. Chou, *Chem. Soc. Rev.* **2010**, *39*, 638.
[4] a) A. Chaskar, H. F. Chen, K. T. Wong, *Adv. Mater.* **2011**, *23*, 3876; b) L. Xiao, X. Xing, Z. Chen, B. Qu, H. Lan, Q. Gong, J. Kido, *Adv. Funct. Mater.* **2013**, *23*, 1323; c) S. Gong, C. Yang, J. Qin, *Chem. Soc. Rev.* **2012**, *41*, 4797.
[5] H. Uoyama, K. Goushi, K. Shizu, H. Nomura, C. Adachi, *Nature* **2012**, *492*, 234.
[6] a) H. Tanaka, K. Shizu, H. Nakanotani, C. Adachi, *Chem. Mater.* **2013**, *25*, 3766; b) J. Li, T. Nakagawa, J. MacDonald, Q. S. Zhang, H. Nomura, H. Miyazaki, C. Adachi, *Adv. Mater.* **2013**, *25*, 3319; c) F. B. Dias, K. N. Bourdakos, V. Jankus, K. C. Moss, K. T. Kamtekar, V. Bhalla, J. Santos, M. R. Bryce, A. P. Monkman, *Adv. Mater.* **2013**, *25*, 3707; d) Q. Zhang, J. Li, K. Shizu, S. Huang, S. Hirata, H. Miyazaki, C. Adachi, *J. Am. Chem. Soc.* **2012**, *134*, 14706.
[7] a) G. Mehes, H. Nomura, Q. S. Zhang, T. Nakagawa, C. Adachi, *Angew. Chem. Int. Edit.* **2012**, *51*, 11311; b) K. Goushi, K. Yoshida, K. Sato, C. Adachi, *Nat. Photonics* **2012**, *6*, 253; c) M. R. Zhu, C. L. Yang, *Chem. Soc. Rev.* **2013**, *42*, 4963.
[8] J. Luo, Z. Xie, J. W. Y. Lam, L. Cheng, H. Chen, C. Qiu, H. S. Kwok, X. Zhan, Y. Liu, D. Zhu, B. Z. Tang, *Chem. Commun.* **2001**, 1740.
[9] a) Y. Hong, J. W. Y. Lam, B. Z. Tang, *Chem. Commun.* **2009**, 4332; b) Y. Hong, J. W. Y. Lam, B. Z. Tang, *Chem. Soc. Rev.* **2011**, *40*, 5361; c) D. Ding, K. Li, B. Liu, B. Z. Tang, *Acc. Chem. Res.* **2013**, *46*, 2441; d) W. Wu, S. Ye, L. Huang, G. Yu, Y. Liu, J. Qin, Z. Li, *Chin. J. Polym. Sci.* **2013**, *31*, 1432; e) C. Li, X. Luo, W. Zhao, Z. Huang, Z. Liu, B. Tong, Y. Dong, *Sci. China Chem.* **2013**, *56*, 1173; f) J. Huang, Q. Li, Z. Li, *J. Mol. Eng. Mater.* **2013**, *01*, 1340006.
[10] a) Z. J. Zhao, J. W. Y. Lam, B. Z. Tang, *J. Mater. Chem.* **2012**, *22*, 23726; b) W. Z. Yuan, P. Lu, S. Chen, J. W. Lam, Z. Wang, Y. Liu, H. S. Kwok, Y. Ma, B. Z. Tang, *Adv. Mater.* **2010**, *22*, 2159; c) Z. J. Zhao, S. M. Chen, J. W. Y. Lam, P. Lu, Y. C. Zhong, K. S. Wong, H. S. Kwok, B. Z. Tang, *Chem. Commun.* **2010**, *46*, 2221; d) Y. Liu, S. M. Chen, J. W. Y. Lam, P. Lu, R. T. K. Kwok, F. Mahtab, H. S. Kwok, B. Z. Tang, *Chem. Mater.* **2011**, *23*, 2536; e) Z. J. Zhao, P. Lu, J. W. Y. Lam, Z. M. Wang, C. Y. K. Chan, H. H. Y. Sung, I. D. Williams, Y. G. Ma, B. Z. Tang, *Chem. Sci.* **2011**, *2*, 672; f) C. Y. K. Chan, Z. J. Zhao, J. W. Y. Lam, J. Z. Liu, S. M. Chen, P. Lu, F. Mahtab, X. J. Chen, H. H. Y. Sung, H. S. Kwok, Y. G. Ma, I. D. Williams, K. S. Wong, B. Z. Tang, *Adv. Func. Mater.* **2012**, *22*, 378; g) W. Z. Yuan, Y. Y. Gong, S. M. Chen, X. Y. Shen, J. W. Y. Lam, P. Lu, Y. W. Lu, Z. M. Wan, R. R. Hu, N. Xie, H. S. Kwok, Y. M. Zhang, J. Z. Sun, B. Z. Tang, *Chem. Mater.* **2012**, *24*, 1518.
[11] a) J. Huang, N. Sun, Y. Dong, R. Tang, P. Lu, P. Cai, Q. Li, D. Ma, J. Qin, Z. Li, *Adv. Func. Mater.* **2013**, *23*, 2329; b) J. Huang, N. Sun, P. Chen, R. Tang, Q. Li, D. Ma, Z. Li, *Chem. Commun.* **2014**, *50*, 2136; c) J. Huang, P. Chen, X. Yang, R. Tang, L. Wang, J. Qin, Z. Li, *Sci. China Chem.* **2013**, *56*, 1213; d) J. Huang, X. Yang, J. Wang, C. Zhong, L. Wang, J. Qin, Z. Li, *J. Mater. Chem.* **2012**, *22*, 2478; e) J. Huang, N. Sun, J. Yang, R. Tang, Q. Li, D. Ma, J. Qin, Z. Li, *J. Mater. Chem.* **2012**, *22*, 12001; f) J. Huang, Y. Jiang, J. Yang, R. Tang, N. Xie, Q. Li, H. S. Kwok, B. Z. Tang, Z. Li, *J. Mater. Chem. C* **2014**, *2*, 2028.
[12] R. Zheng, M. Häussler, H. Dong, Jacky W. Y. Lam, B. Z. Tang, *Macromolecules* **2006**, *39*, 7973.
[13] Y. Dong, J. W. Y. Lam, A. Qin, J. Liu, Z. Li, B. Z. Tang, J. Sun, H. S. Kwok, *Appl.Phys. Lett.* **2007**, *91*, 011111.
[14] J. Huang, X. Yang, X. Li, P. Chen, R. Tang, F. Li, P. Lu, Y. Ma, L. Wang, J. Qin, Q. Li, Z. Li, *Chem. Commun.* **2012**, *48*, 9586.